# XMM-Newton Calibration Technical Note

## XMM-SOC-CAL-SRN-0391

## Spatial CTI correction and energy scale in [6,9] keV for XMM-Newton EPIC-pn in Full Frame and Extended Full Frame modes

Ivan Valtchanov (XMM-SOC, ESAC), SCO-04, WA4200

October 25, 2022

# 1    CCF components

| Name of CCF | VALDATE | EVALDATE | Blocks changed | CAL version | XSCS flag |
|---|---|---|---|---|---|
| EPN_SPATIALCTI_0001.CCF | 2000-01-01T00:00:00 | | MN_SPATIALCTI CU_SPATIALCTI | 3.256 | NO |

# 2    Summary

Using stacked events lists, following Sanders et al. (2020) (S20 from now on), we derive time-dependent spatial corrections for EPIC-pn based on the Cu Kα fluorescent line at 8 keV and at 6 keV using the Mn Kα line from the calibration source.

The offsets are incorporated into a new calibration file `EPN_SPATIALCTI_0001.CCF`, and the XMM-SAS task `epspatialcti` is modified in a way that it can be used with this file to correct the energies of the events.

The spatial homogeneity of Cu Kα, after applying the correction of Cu Kα, increases on average by a factor of ∼ 6 for FF, and a factor of ∼ 4 for EFF. Applying the Cu Kα-derived offsets for the Mn Kα line at 6 keV in FF, however, shows only a marginal improvement.

The analysis of the energy scale of six instrumental lines in the [6,9] keV range: Mn Kα, Mn Kβ,

Ni K$\alpha$, Zn K$\alpha$, Cu K$\alpha$ and Cu K$\beta$ does not indicate an obvious time dependence as in S20. Because the deviations are small and the secondary effects of this correction are not clear, we do not see a strong justification to implement an energy-scale compression or stretch at this stage.

# 3    Introduction

We follow S20 where they introduced a three-stage correction procedure in order to improve the energy scale of EPIC-pn. The technique is then used to measure bulk flows in the intra-cluster medium of the Perseus and Coma clusters (S20), and more recently for the Virgo (Gatuzz et al., 2022a) and Centaurus clusters (Gatuzz et al., 2022b). Because of the potential benefit of this improvement, the XMM SOC decided to derive and implement a similar three-step procedure and produce calibration files and XMM-SAS tools necessary for its use by the community.

# 4    First-step correction

The first-step correction is part of the long-term CTI update as reported in Valtchanov & Smith (2022). After processing the event lists, the offset per-CCD of the Cu K$\alpha$ line from the lab energy should be zero within the uncertainties of the derived correction. Unlike S20, the long-term CTI correction is per CCD and not for the full EPIC-pn (excluding the copper hole).

# 5    Second-step correction

The second-step correction uses events already corrected for the overall long-term CTI per CCD (Step 1). We will use the spatial offsets of the best-fit line energy of Cu K$\alpha$ derived from spectra extracted for each read-out column (RAWX) and in bins of 20 RAWY pixels for each CCD. To increase the statistics, the events will be stacked in bins of 500 XMM-Newton revolutions prior to the spectral extraction.

## 5.1    Stacking procedure

For all FF and EFF mode observations we stack the events in bins of 500 revolutions. As in S20, for redundancy, we consider two sets of stacked event lists:

- Stack set 1: $[1, 500), [500, 1000), \cdots, [3500, 4000)$

- Stack set2: $[250, 750), [750, 1250), \cdots, [3750, 4250)$

We have stack sets for all 12 CCDs and considered only single events (`PATTERN==0`) with energies from 5.5 to 10 keV.

## 5.2    Spectral extraction

We extract spectra for each CCD for all 64 read-out columns (RAWX) and in bins of 20 RAWY columns. As the first 12 RAWY pixels are not used, keeping the first bin from RAWY=1 to RAWY=20 will only have 8 pixels to use, which will make it unusable for spectral fit. Therefore we merged this bin with the next one, hence the first binned spectrum starts at RAWY=12 and ends at RAWY=40. The next one starts at RAWY=41 and ends at RAWY=60, etc. The last bin is from RAWY=181 to RAWY=200.

The extracted spectra are then binned in spectral bins of 5 eV. Each extracted spectrum covers energies in [5.5,10] keV.

We exclude bins that fall into a region around the boresight where the $\mathrm{Cu\,K\alpha}$ fluorescence is not present (the copper hole). Here are the conditions for the excluded regions:

- CCDNR in 4 or 10: RAWX $\leq$ 20 and RAWY $\geq$ 140; RAWX $>$ 20 and RAWY $\geq$ 120;

- CCDNR in 1 or 7: RAWX $\leq$ 40 and RAWY $\geq$ 120; RAWX $>$ 40 and RAWY $\geq$ 140;

## 5.3    Spectral fit for $\mathrm{Cu\,K\alpha}$

To obtain the best-fit $\mathrm{Cu\,K\alpha}$ line energy, we use `astropy.modeling` to fit a single `Gaussian1D` line and a second-order polynomial continuum, with Levenberg-Marquardt algorithm and least squares statistic.

Note that our experiments with fitting a 4-line model around the $\mathrm{Cu\,K\alpha}$ line (see next section) did not show significant differences for the best-fit line energy (within $\pm 1$ eV) and therefore we considered only a single Gaussian model for $\mathrm{Cu\,K\alpha}$.
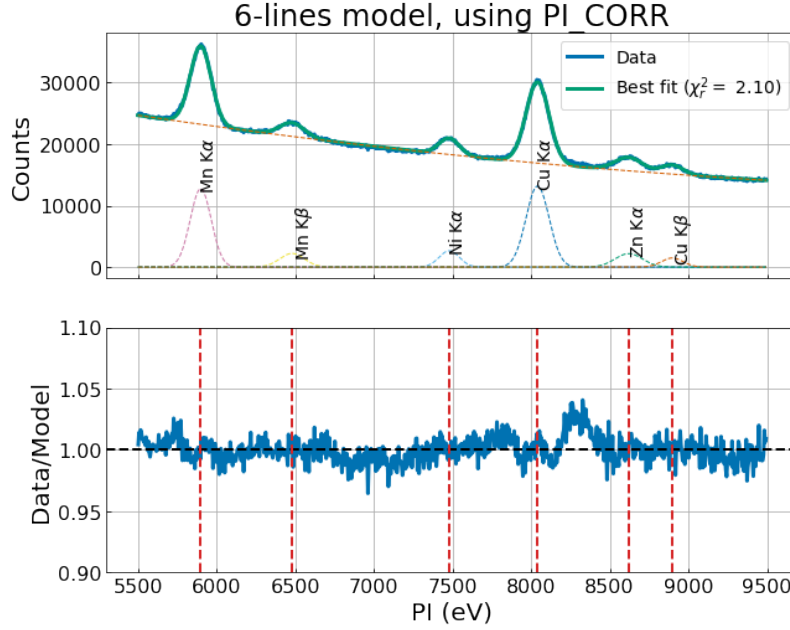
Figure 1: Illustration of the 6 lines included in the energy scale analysis. The spectrum is extracted from the full CCD area after applying the Cu Kα-derived spatial offsets.

## 5.4    Spectral fit for energy scale

For the analysis of the energy scale from 6 to 9 keV we consider the following six instrumental lines: Mn Kα (5.8956 keV)[1], Mn Kβ (6.49 keV), Ni Kα (7.470 keV), Cu Kα (8.038 keV), Zn Kα (8.630 eV) and Cu Kβ (8.90 keV). And an example of a spectrum with the six lines is shown in Fig. 1

The two manganese lines are from the internal iron-55 calibration source and are only available in *CalClosed* observations. Therefore we extracted stacked event lists only for observations in this mode in order to fit the lines. During early epochs after the XMM-Newton launch (e.g., rev. < 1000) the iron-55 calibration source is quite strong and the Mn Kα line dominates. With its half-life of 2.737 years, the cal source becomes fainter and fainter, and it is barely possible to fit the Mn Kα line for the stacked spectra after revolution 2500.

Based on these considerations, we fit two separate models for the two datasets: 2-line model for Mn Kα and Mn Kβ using stacks with *CalClosed* data only and 4-line model for Ni Kα, Cu Kα, Zn Kα and Cu Kβ lines using all stacked events, including *CalClosed* ones.

---

[1]The adopted line energy of 5.8956 keV for Mn Kα is the centroid of Mn Kα$_1$ at 5.8876 keV (weight 0.5) and Mn Kα$_2$ at 5.8988 keV (weight 1.0), convolved with the pn response.

## 5.5    Deriving the spatial offsets and storing them in a calibration file

The difference in the best-fit line energy in each spatial bin with the expected energy of Cu Kα gives the offset and its uncertainty from the fit uncertainty on the best-fit line energy. For each CCD we have $64 \times 8$ spatial bins, we also have 8 epochs with 500 revolution bins for the two stack sets. With the overlap of the stack sets, we can create an average correction on a grid of 250 revolutions over 17 epochs, with the first and last epochs the non-averaged values as there is no overlap.

The calibration file `EPN_SPATIALCTI_0001.CCF` contains the spatial CTI offsets stored in a 3-dimensional array `MDELTA` with dimensions (12,64,200) for each of the two observing modes: Full Frame (`MODE_ID=0`) and Extended Full Frame (`MODE_ID=1`) and for each of the 17 epochs with a step of 250 revolutions. `MDELTA` is the average correction of the two stack sets, and we also provide the 3-D `MDELTA_ERR` with the correction error taken as the quadrature error of the two stack sets correction errors. Note that, for convenience, we expanded the original 8 RAWY bins to the full 200 RAWY pixels. Due to the spatial distribution of Cu Kα, the offsets in the copper hole are set to zero (see Sect. 5.2).

For an event list in a given observations, the XMM-SAS task `epspatialcti` selects the corresponding spatial CTI offset 3-D table `MDELTA` (CCDNR,RAWX,RAWY) with the observing mode (0 for FF or 1 for EFF) and taking the revolution bin where the observation falls, for example, for an FF observation during revolution 1205, the selected `MODE_ID = 0`, `EPOCH=int(1205/250)=4`. Following S20, we apply the derived offsets `MDELTA` to the input event energy (PI column) as follows:

$$\mathrm{PI\_CORR} = \mathrm{PI} + rand() - \mathrm{MDELTA}, \tag{1}$$

where we randomise the PI values by adding a random number in $[0, 1)$.

Event lists that were corrected witht the spatial CTI correction XMM-SAS task `epspatialcti` have the keyword `SPATCTIC` set to `True`.

# 6    Results

## 6.1    Spatial offsets for Cu Kα, before and after

An example of the derived spatial offsets for Cu Kα for stacked event lists for rev. in $[1000, 1500]$ are shown in Fig. 2, left panel. After correcting the energies of the events and following the same spectral extraction and line fitting, we obtain the spatial residuals as shown in Fig. 2, right panel. We see a significant improvement of the st.dev. of the spatial residuals by a factor of 10 (see also Table 2).
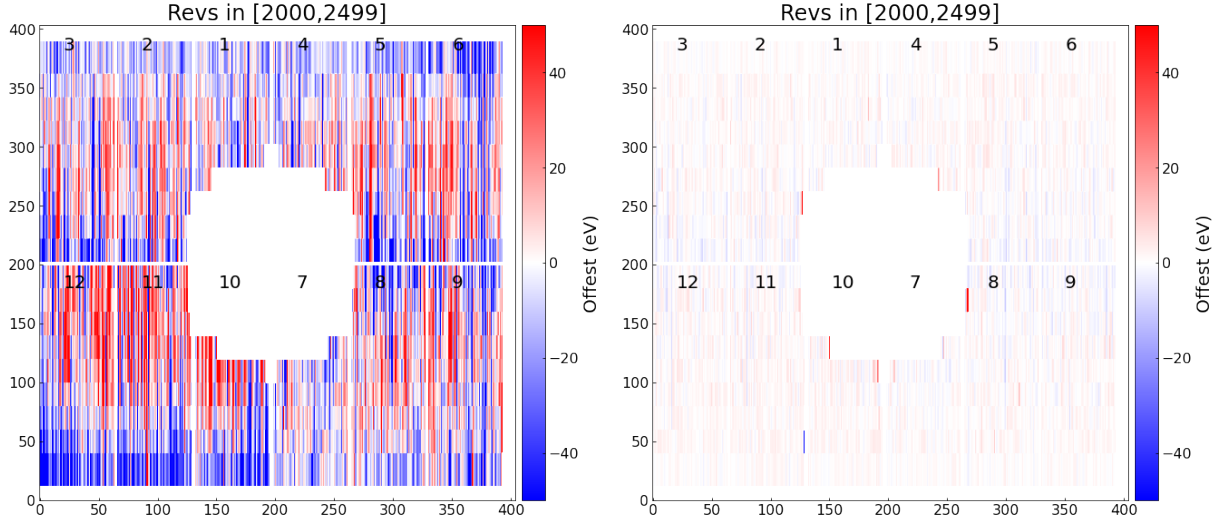
Figure 2: Example of $Cu\,K\alpha$ spatial residuals before (left) and after (right) applying the correction, for FF mode and revolution bin $[2000, 2500)$. Note that the offset is derived from the left panel, then applied on the stacked events before these are extracted in spectra and the $Cu\,K\alpha$ line is fit.

Combining all epochs and CCDs, the comparison before and after for the FF mode is shown in Fig. 3 and for the EFF in Fig. 7. The before and after mean results tabulated in Tables 2 and 3. We see a significant decrease in the st.dev. and also removing the time-dependent increase in the spatial inhomogeneity across the pn detector.

If we consider the residual st.dev. ($rms$) across the pn detector as the residual uncertainty on the redshift of a spectral line, we can convert this to the velocity uncertainty via:
$1 + z = E_{emit}/E_{obs} = E_{emit}/(E_{emit} - rms)$ and then $\Delta v = c \times z$.

In the case of $Cu\,K\alpha$, with an offset of the order of 25 eV before and 4 eV after correction, we obtain $\Delta v \approx 950$ km/s before and $\Delta v \approx 150$ km/s after[2].

## 6.2   Spatial offsets for $Mn\,K\alpha$, before and after

In S20, the derived offsets from $Cu\,K\alpha$ were used to correct events with energies down to 6 keV (Sanders, private communication). We decided to test whether applying the $Cu\,K\alpha$-derived offsets would improve the spatial residuals at 6 keV using as a test $Mn\,K\alpha$.

An example comparison of before and after applying the $Cu\,K\alpha$-derived offsets for $Mn\,K\alpha$ is shown in Fig. 4, we used stacks of only CALCLOSED observations.

---

[2]As a general rule, $rms$ of 10 eV at 8 keV, which corresponds to $\Delta v$ of 375 km/s. At 6 keV the same $rms$ of 10 eV corresponds to $\Delta v$ of 500 km/s.
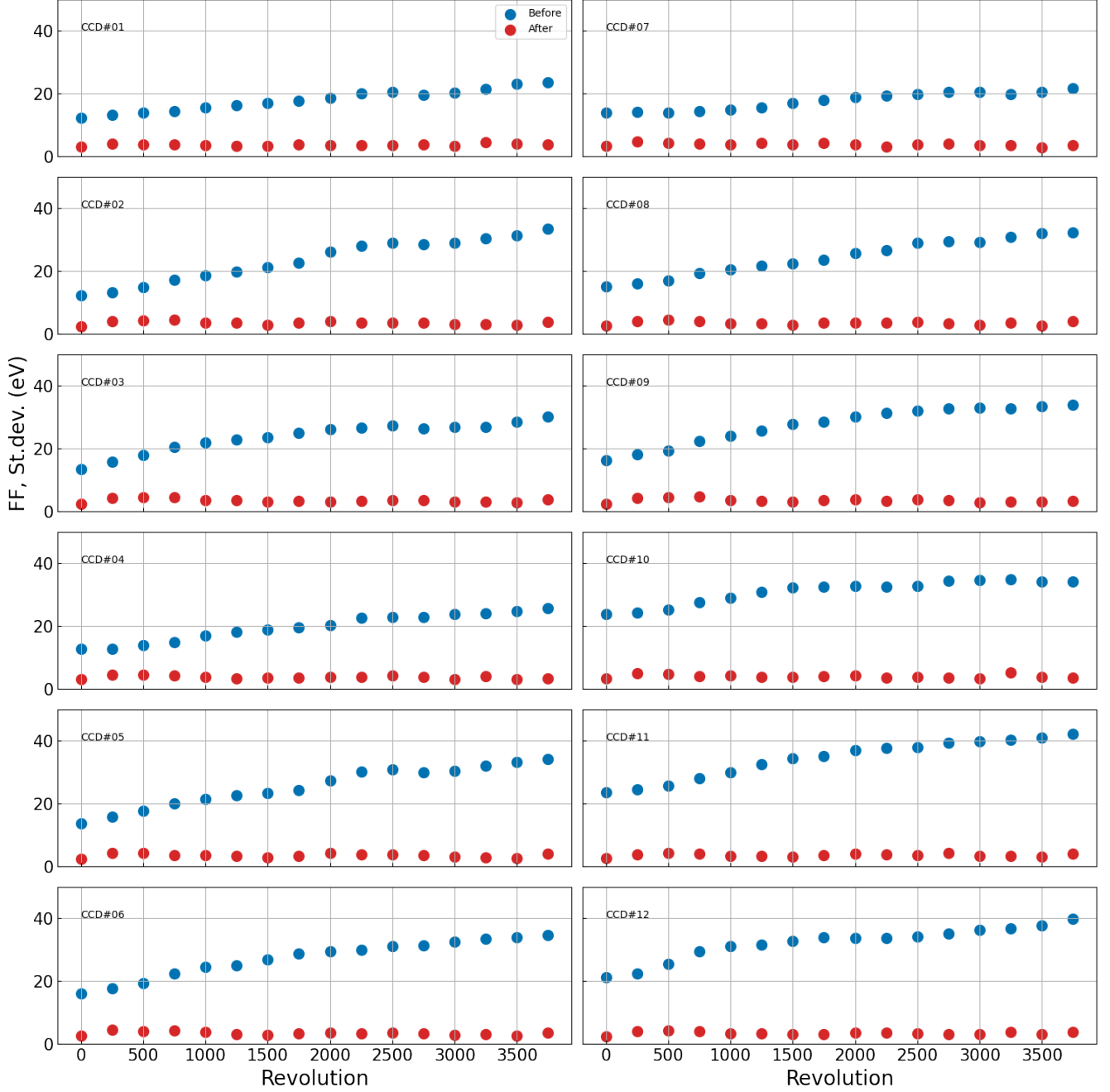
Figure 3: The st.dev. of the Cu Kα residuals before (blue) and after (red) applying spatial offsets. Full Frame mode results for all CCDs and all 16 epochs, note that the points, except the first and last ones, are not statistically independent due the overlap of 250 revolutions for stack set 1 and stack set 2. The mean values per CCD are shown in Table 2 for FF mode.
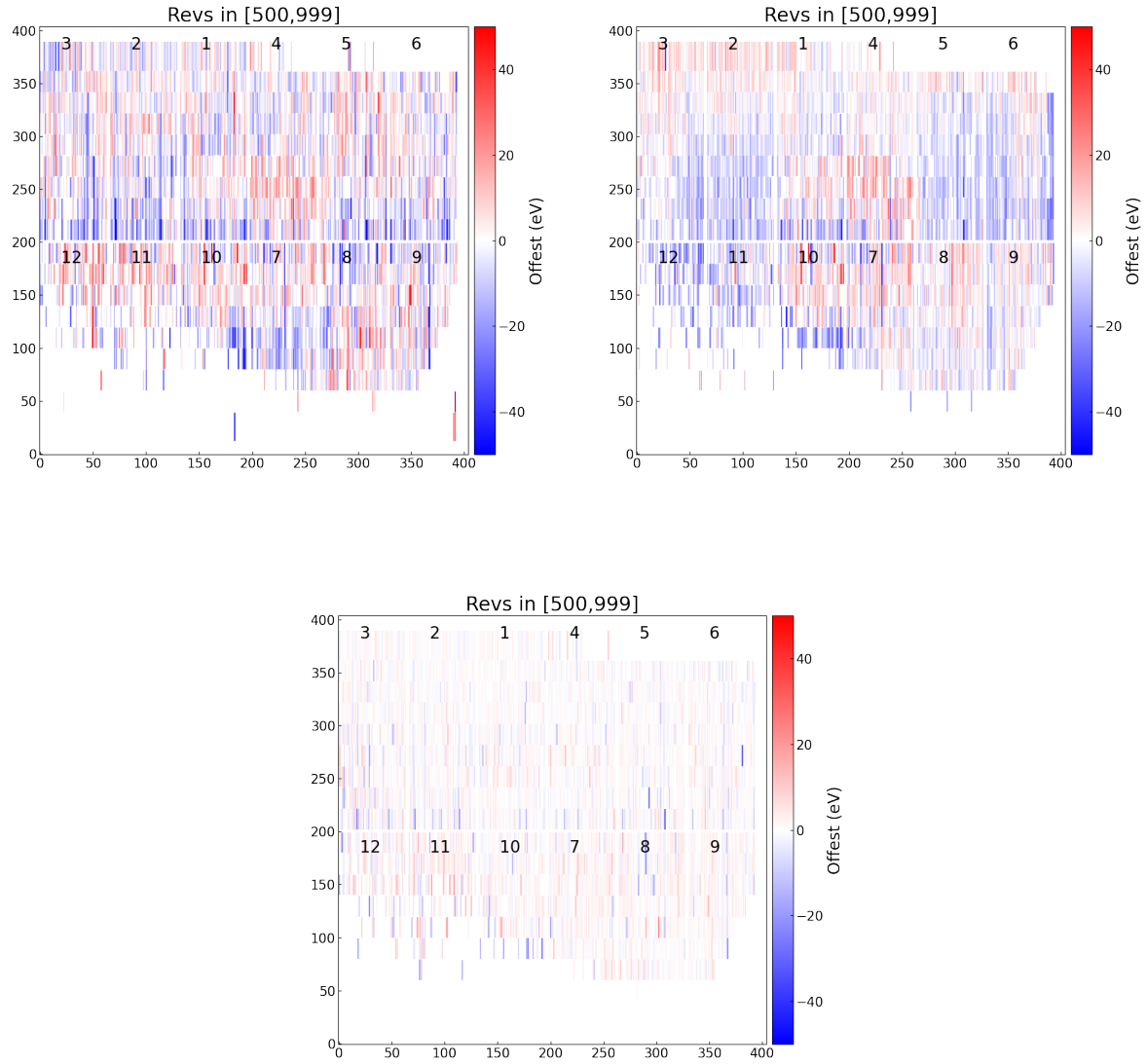
Figure 4: Example of Mn Kα spatial residuals before (left) and after applying the Cu Kα correction (right) and after applying the Mn Kα correction (bottom), for FF mode and revolution bin [500, 1000). The same colour scale is used in the three panels. Note that the correction is applied at an event list level, before these are extracted in spectra and the Mn Kα line is fit.

Note the very different spatial distribution of $\mathrm{Mn\,K\alpha}$ as compared to $\mathrm{Cu\,K\alpha}$, and also the characteristic low illumination of quadrants 3 and 4 (CCDs 7 to 12) from the cal source. The region in the centre, in the copper hole, is not corrected.

Fig. 5 shows the results for all epochs and CCDs for FF mode and indicates marginal but systematic improvement in the spatial residuals for $\mathrm{Mn\,K\alpha}$ as quantified by the st.dev. There is also a noticeable small increase in the st.dev. even after applying the spatial offsets.

Assuming the observed residuals as velocity uncertainty, as in the previous subsection, we can see a marginal improvement from $rms$ of 18 eV (excluding quadrant 4) to 13 eV, which corresponds to $\Delta v \approx 900$ km/s before to $\Delta v \approx 650$ km/s after (see Table 4).

Concluding, we have validated that applying the $\mathrm{Cu\,K\alpha}$-derived spatial offsets leads to small systematic improvements of the spatial homogeneity at 6 keV for all CCDs and epochs. Therefore we can use the correction to events with energies down to 6 keV. However, validation with the $\mathrm{Mn\,K\alpha}$ line indicates a factor of 5 larger $\Delta v$ compared to $\mathrm{Cu\,K\alpha}$, and it is likely that the same order of uncertainty is expected for the Fe K complex at 6.4 keV.

# 7    Spatial offsets using $\mathrm{Mn\,K\alpha}$ line

In principle, we could use the spatial residuals derived from $\mathrm{Mn\,K\alpha}$ (Fig. 4, left panel) and implement a correction in a similar way. Using the $\mathrm{Mn\,K\alpha}$ spatial residuals to correct event energies has its benefits: it is closer to the putative energy of the iron-line complex at 6.5 keV in sky sources and also the spatial correction can be derived for the region around he boresight. There are, however, some drawbacks: the signal-to-noise ratio for the spatial bins decreases with time as the calibration source decays and parts in quadrant 4 (CCDs 10, 11,12) are poorly illuminated. Up to rev. bin [2000,2500) the number of successful fits is still acceptable, but afterwards there is only a small number of spatial pixels with good results. Different spatial binning could alleviate this problem of signal-to-noise ratio, e.g. by binning more read-out columns. Unfortunately, nothing can be done for the poorly illuminated part of quadrant 4.

An example of one stack with $\mathrm{Mn\,K\alpha}$ after applying the $\mathrm{Mn\,K\alpha}$-derived spatial correction is shown in Fig. 5, bottom panel.

The general comparison with the results corrected for $\mathrm{Cu\,K\alpha}$ for all epochs and CCDs is shown in Fig. 5. We see a significant improvement with respect to the $\mathrm{Cu\,K\alpha}$ corrected results, although after revolution 2000 the two are similar. The quantitative comparison of the two corrections is shown in Tab. 4.

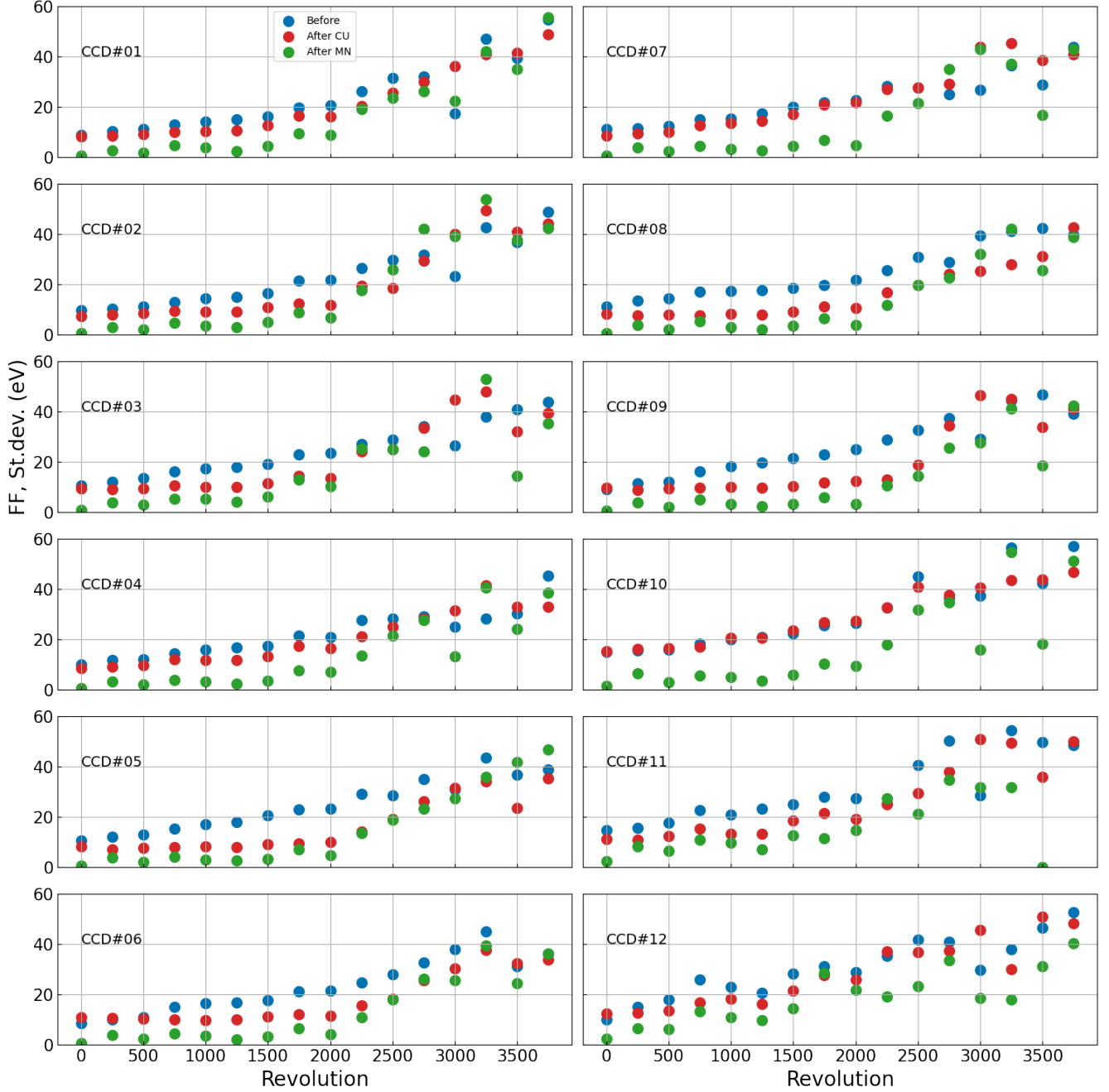Due to the scarcity of *CalClosed* EFF observations, we cannot derive a correction for this mode.

Figure 5: The st.dev. of the Mn Kα residuals before and after applying the Cu Kα-derived spatial offsets (red) and Mn Kα-derived correction (green). Full Frame mode results for all CCDs and all epochs. The mean values per CCD are shown in Table 4 for FF mode.

Table 1: Full Frame mode, CCD02, revs in $[2000, 2500)$ results.

| set | mean | median | st.dev. |
|---|---|---|---|
| Stack 1/2 before | -1.7 | -1.2 | 26.4 |
| Stack 2/2 before | -0.7 | -0.7 | 26.2 |
| Stack 1/2 corr 1 | 0.06 | 0.1 | 1.4 |
| Stack 1/2 corr 2 | -0.5 | -0.03 | 7.1 |
| Stack 2/2 corr 1 | 0.4 | 0.3 | 6.8 |
| Stack 2/2 corr 2 | 0.02 | 0.07 | 1.4 |

# 8    Validation with independent stack split

The stacking strategy with two sets of stacks shifted by 250 revolutions should provide in principle sufficient randomness, so that we could consider the two offsets as independent. Nevertheless, we checked this assumption by taking a 500 revolution stack, splitting it into two independent sets by random choice of observations (without duplications) and deriving two sets of independent corrections. We then apply the fist correction on both the first and the second set and vice versa. As this is a consistency check we only used one CCD – CCDNR 02 and one 500 revolutions stack – revs in $[2000, 2500)$. The results are shown in Table 1.

The validation clearly demonstrates that applying the correction from an independent list of events leads to similar improvements in the st.dev. of the spatial residuals as those reported in Table 2, a factor of $\sim 4$. Note that it is expected the st.dev. in this experiment is larger as the number of events is smaller (stack of 250 revolutions instead of 500) and hence the uncertainties in the best-fit $Cu\,K\alpha$ centroid are larger.

It also demonstrates that using non-independent events the improvement is much more significant, i.e. from st.dev. of 26 eV to 1.4 eV. This is clearly not the case when we combine the two sets of stacks.

# 9    Third-step correction: energy scale between 6 and 9 keV

In S20, the authors modelled a time-dependent energy scale stretch (or compression) for the energies of the lines around $Cu\,K\alpha$. We investigated this problem with stacked event lists after applying spatial offsets. We consider the composite 2-lines (only from *CalClosed* observations) and 4-lines models in this analysis.

In S20, they binned each CCD in 8 pixels: 4 bins on RAWX (16 read-out columns combined) and 2 bins in RAWY (100 pixels) and stacked in bins of 250 revolutions. Our attempts to fit the 6
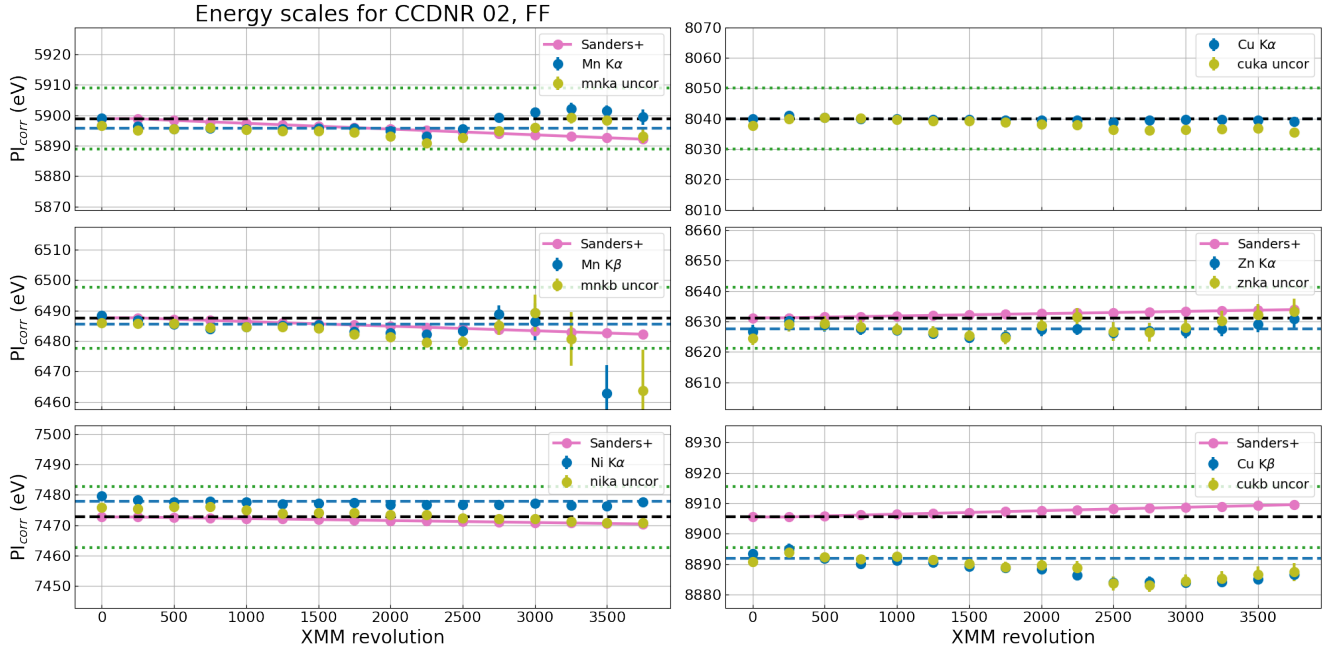
Figure 6: An example of the energy scale for CCDNR02 in FF mode, after applying the second-step correction (spatial CTI). The data points (blue dots) are the best-fit line energies after the spatial CTI correction, olive points are before the correction. The black dashed line is the reference line energy, the blue dashed line is the median of the fitted line energies using the first 5 stacks data points (rev $\leq$ 1000), the green dotted lines are at $\pm 10$ eV around the reference energy of the line. The S20 time-dependent energy scale correction, averaged for the full CCD area, is shown with pink curves. Note that the data points (blue and olive dots) are not statistically independent as there is 250 revolution overlap, except for the first and the last ones.

lines with such spectral extraction from the 8 stacked spatial bins were hugely uncertain: in most cases the fitting was not converging or the fitted parameters were with large uncertainties, e.g. larger than 50 eV on line centroids. Hence, for this analysis we used stacked spectra extracted from the full CCD areas with the 500 revolution bins in the two stack sets.

The results for CCDNR02 are shown in Fig. 6 for FF mode, while the rest of the CCDs are shown in the appendix C and for EFF mode in appendix D.

There is a lot of information in those figures and here we summarise some obvious observations:

- Cu Kα results should be consistent with zero offset with respect to the lab energy of the line.

- The Mn Kα line results do not show large deviations from the expected energy, except for CCDNR04 where the long-term CTI for this line is optimised for the boresight only. Some recent epochs show some deviation at around 10 eV, which is understood to be due to the modelling of the CTI using individual observations, whereas the results here are produced with stacked event lists.

- For EFF, since we have a few observations *CalClosed*, the results for $Mn\,K\alpha$ and $Mn\,K\beta$ are much more uncertain.

- There is dramatic improvement for $Ni\,K\alpha$ line after applying the spatial CTI: it shows small constant offsets of $\sim 5$ eV for both FF and EFF for all CCDs. While th euncorrected results show systematic constant offset at $\sim 10$ eV.

- $Zn\,K\alpha$ behaviour is with no obvious pattern: for some CCDs it is flat and small ($<5$ eV) and for others its flat at $\sim 10$ eV.

- $Cu\,K\beta$ best fit energy after the correction is systematically at lower energies by $\sim 10$ eV. This is to be expected, as the long-term CTI for events with energies above 8 keV are corrected with the same constant correction as for $Cu\,K\alpha$.

- The results in quadrant 3 (CCDNRs 10, 11 and 12) are the most uncertain ones, especially for EFF mode. This quadrant is not properly illuminated by the cal source and therefore the long-term CTI correction is uncertain and this reflects on the results. For the cal source lines it was not possible to derive the best-fit line energies for EFF mode and CCDNR 11 and 12.

In summary: based on these results, in principle we could derive an empirical energy correction for the events with energies of 6 to 9 keV. We have to note that the deviations are small ($\lesssim 10$ eV) and in the majority of the cases, without obvious time-dependent patterns. Moreover, they are discrepant with the S20 derived corrections (slope and offset). We cannot guarantee that incorporating such an empirical energy offset, derived from stacked spectra, would not introduce some unknown secondary effects when it is applied on individual observations. Therefore, we do not see a strong case to implement it at this stage.

# 10    Conclusions

Using the fluorescent $Cu\,K\alpha$ line at 8 keV and the $Mn\,K\alpha$ line at 6 keV from the calibration source we derived residuals on a spatial grid for each CCD for EPIC-pn for FF. For the EFF mode we only have the $Cu\,K\alpha$ derived results due to the scarcity of *CalClosed* observation in this mode. We stacked event lists with events energies already corrected for the long-term CTI with the latest update, as implemented in CAL-SRN-0389. The stacked event lists allow for spectral extraction and fit for the $Cu\,K\alpha$ and $Mn\,K\alpha$ lines in spatial bins along all read-out columns (RAWX) and in bins of 20 RAWY pixels. Applying the offsets on the initial stacked event lists and re-deriving the best-fit line energy we see a significant improvement in the spatial residuals, a factor of $\sim 6$ decrease in the st.dev. of the $Cu\,K\alpha$ residuals for FF and a factor of $\sim 4$ decrease for EFF. Interpreting this st.dev. as the uncertainty on redshift and in velocity space this leads to a significant decrease from $\Delta\upsilon \approx 1000$ km/s to $\sim 150$ km/s across the EPIC-pn detector (excluding the copper hole) at 8 keV.

Applying the $Cu\,K\alpha$ offsets at lower energies, e.g. at 6 keV, lead to marginal improvements in the spatial residuals for the $Mn\,K\alpha$ line. Nevertheless, this small improvement is observed for all

CCDs and epochs. Deriving and applying Mn Kα offsets improves significantly the Mn Kα spatial residuals, although within certain limits: the low signal-to-noise ratio of the cal source line for observations after revolution 2000 leads to large uncertainties and too many spatial bins with failed fit for the centroid. And not having enough *CalClosed* observations in the EFF mode leads to impossible fit for the line with the adopted stacking strategy and spatial binning.

The main goal of the spatial CTI correction is to allow for a better characterisation of the 6.5 keV iron line complex in astronomical sources, i.e. to have better control on the systematics of the velocity structures in different spatial regions, as was done in Sanders et al. (2020); Gatuzz et al. (2022a,b). In practical terms, we demonstrated that applying the Cu Kα offsets to the 6 keV instrumental line leads to a marginal improvement and does not cover the boresight area. Applying the offsets derived from Mn Kα is more promising, as it is closer to the 6.5 keV line and also includes the boresight region. However, it is only good for observations before revolution 2000 and in FF mode. The two corrections based on Cu Kα and Mn Kα are available through the XMM-SAS task `epspatialcti`, and the interested users could check the results with both corrections for their observations.

The energy scale analysis of the six instrumental lines in energy range from 6 to 10 keV, after we apply spatial CTI correction, show different behaviours for the different lines for FF and EFF and depending on the CCD. We cannot see any systematic patterns and this will complicate the derivation of an empirical time-dependent correction. In many cases, we see a different behaviour (slope and offset) compared to the S20-derived energy scale corrections. Therefore, taking into account all these arguments, we do not consider implementing a third step empirical energy scale correction at E > 6 keV at this stage.

The results with the 6-lines modelling of the energy scale may be used to re-derive and improve the long-term CTI using stacked event lists on more than the three reference energies (Al Kα, Mn Kα and Cu Kα), by including, e.g. Ni Kα, Zn Kα and Cu Kβ lines.

# 11    Practical considerations

The user should be aware that there are a number of caveats to take into account when applying the spatial correction derived from the Cu Kα or Mn Kα lines.

- The correction, as implemented in `epspatialcti`, is applied on all energies (PI). The average spatial offset is of the order of 20 eV, which is 0.25% in relative terms at 8 keV, 0.33% at 6 keV, and 1.33% at 1.5 keV.

- The Cu Kα-derived correction is zero (i.e. no correction) for all events within the copper hole: a region of radius $\sim 6.5'$ centred on the boresight.

- Quadrant 4 (CCDs 10, 11 and 12) is poorly illuminated by the calibration source; hence, there is no Mn K$\alpha$-based correction for this area.

- The calibration source (iron-55) decays and the signal-to-noise ratio for the Mn K$\alpha$ line becomes too low in the stacked events after revolution bin [2000,2500), hence most spatial pixels will have zero correction.

# 12    Further work

Using the derived offsets we shall compare with the S20 results of the velocity structure of Perseus (and ideally other sources). It will be informative to compare the outcome for the same spatial regions when applying the Cu K$\alpha$ or Mn K$\alpha$ corrections.

# References

Gatuzz, E., Sanders, J. S., Dennerl, K., et al. 2022a, MNRAS, 511, 4511, doi: 10.1093/mnras/stab2661

Gatuzz, E., Sanders, J. S., Canning, R., et al. 2022b, MNRAS, 513, 1932, doi: 10.1093/mnras/stac846

Sanders, J. S., Dennerl, K., Russell, H. R., et al. 2020, A&A, 633, A42 (S20), doi: 10.1051/0004-6361/201936468

Valtchanov, I., & Smith, M. J. S. 2022, XMM-Newton EPIC-pn: long-term CTI update, Tech. Rep. XMM-CCF-REL-389, XMM SOC

# A    Results for st.dev. before and after

As a general rule, *RMS* of 10 eV at 8 keV corresponds to $\Delta v$ of 375 km/s. At 6 keV the same *RMS* of 10 eV corresponds to $\Delta v$ of 500 km/s.

Table 2: Time-averaged results for st.dev. for FF mode and Cu K$\alpha$. Note that the st.dev. is calculated after iterative removal of 3-$\sigma$ outliers.

| CCD# | Before (eV) | After (eV) | CCD# | Before (eV) | After (eV) |
|---|---|---|---|---|---|
| 01 | 18.0 | 3.8 | 07 | 17.7 | 3.9 |
| 02 | 23.5 | 3.6 | 08 | 24.5 | 3.6 |
| 03 | 23.8 | 3.5 | 09 | 27.7 | 3.6 |
| 04 | 19.7 | 3.8 | 10 | 31.0 | 4.1 |
| 05 | 25.5 | 3.5 | 11 | 34.4 | 3.7 |
| 06 | 27.4 | 3.5 | 12 | 32.2 | 3.5 |

Table 3: Tme-averaged results for st.dev. for EFF mode and Cu K$\alpha$. Note that the st.dev. is calculated after iterative removal of 3-$\sigma$ outliers.

| CCD# | Before (eV) | After (eV) | CCD# | Before (eV) | After (eV) |
|---|---|---|---|---|---|
| 01 | 27.3 | 9.3 | 07 | 31.6 | 9.7 |
| 02 | 31.2 | 8.2 | 08 | 37.5 | 9.1 |
| 03 | 30.0 | 7.7 | 09 | 44.7 | 9.1 |
| 04 | 29.3 | 9.4 | 10 | 49.6 | 9.7 |
| 05 | 36.7 | 7.9 | 11 | 68.8 | 9.3 |
| 06 | 42.7 | 7.6 | 12 | 57.5 | 9.1 |
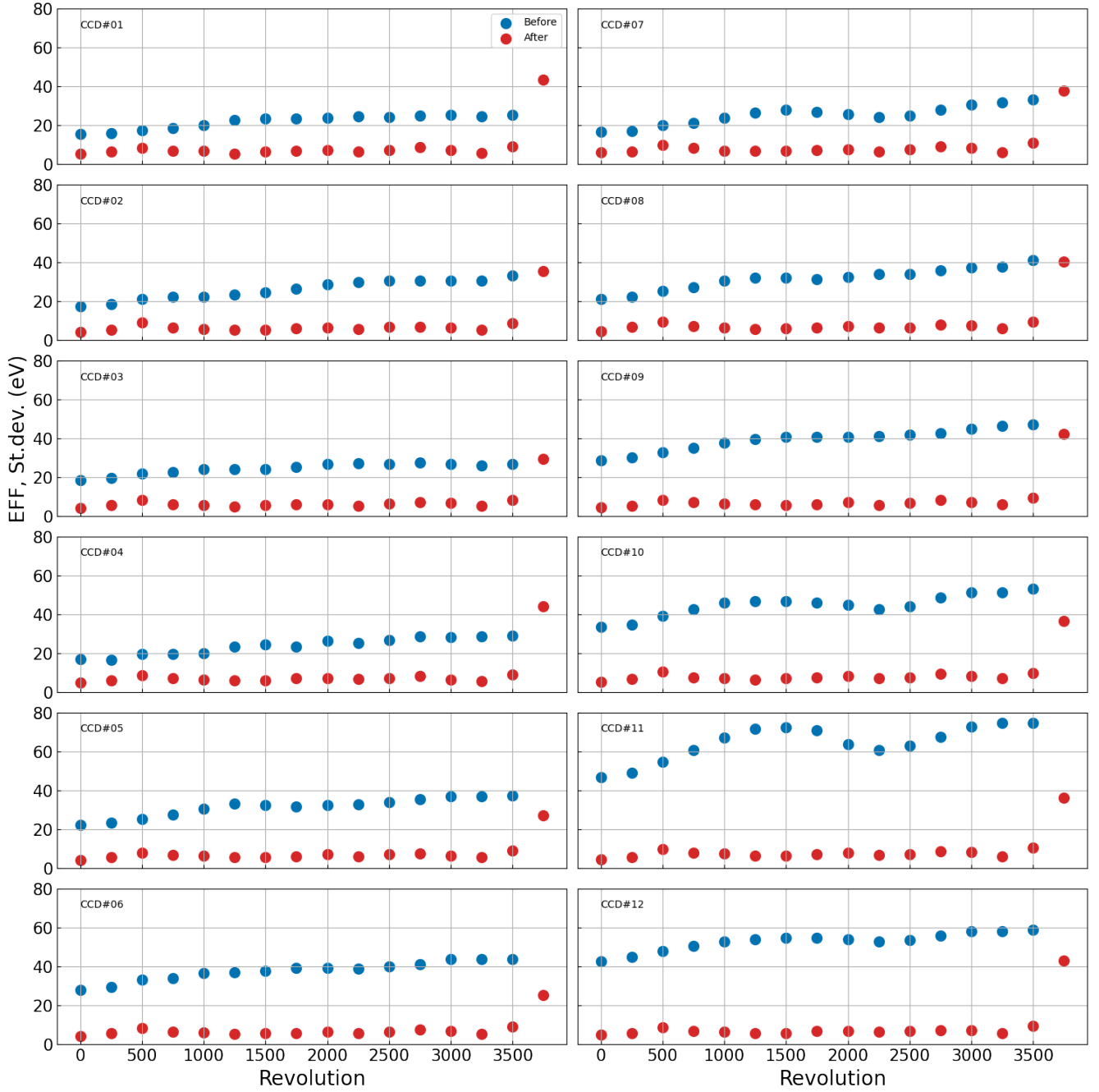
Figure 7: The st.dev. of the Cu Kα residuals before (blue) and after (red) applying spatial offsets. Extended Full Frame mode results for all CCDs and all 16 epochs, note that the points, except the first and last ones, are not statistically independent due the overlap of 250 revolutions for stack set 1 and stack set 2.

Table 4: Results for st.dev. for FF mode and $\mathrm{Mn\,K\alpha}$ after the $\mathrm{Cu\,K\alpha}$ and $\mathrm{Mn\,K\alpha}$ derived corrections. Note that the st.dev. is calculated after iterative removal of 3-$\sigma$ outliers and only considering stacks up to revolution 2000.

| CCDNR | Before | After $\mathrm{Cu\,K\alpha}$ (eV) | After $\mathrm{Mn\,K\alpha}$ | CCDNR | Before | After $\mathrm{Cu\,K\alpha}$ (eV) | After $\mathrm{Mn\,K\alpha}$ |
|-------|--------|----------------|----------------|-------|--------|----------------|----------------|
| 01 | 14.5 | 11.4 | 4.4 | 07 | 16.4 | 14.4 | 3.8 |
| 02 | 14.9 | 9.7 | 4.3 | 08 | 16.9 | 8.8 | 3.5 |
| 03 | 17.2 | 11.0 | 5.9 | 09 | 17.5 | 10.3 | 3.4 |
| 04 | 15.7 | 12.3 | 3.8 | 10 | 20.1 | 20.5 | 5.7 |
| 05 | 17.0 | 8.5 | 3.5 | 11 | 15.2 | 15.2 | 9.4 |
| 06 | 15.4 | 10.8 | 3.4 | 12 | 22.4 | 18.4 | 12.7 |

# B    Temporal variation of the $\mathrm{Cu\,K}\alpha$ derived spatial CTI corrections

The variation with time of the $\mathrm{Cu\,K}\alpha$-derived spatial CTI correction for an arbitrary choice of CCD and a few pixels are shown in Fig. 8.
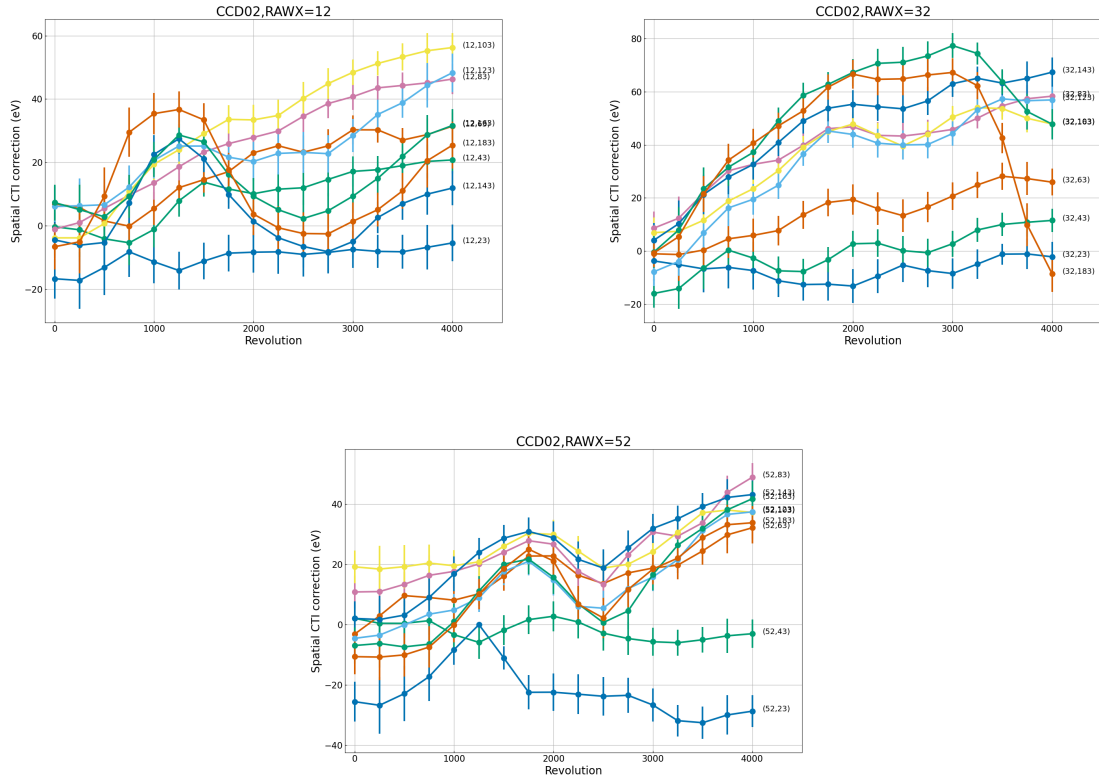


Figure 8: The time dependence of the $\mathrm{Cu\,K}\alpha$-derived correction for CCDNR02 and some arbitrary selected RAWY pixels (annotated curves) for an arbitrary selection of read-out columns: RAWX=11 (top left), RAWX=31 (top right) and RAWX=51 bottom.

# C   Energy scale results for FF mode and all CCDs
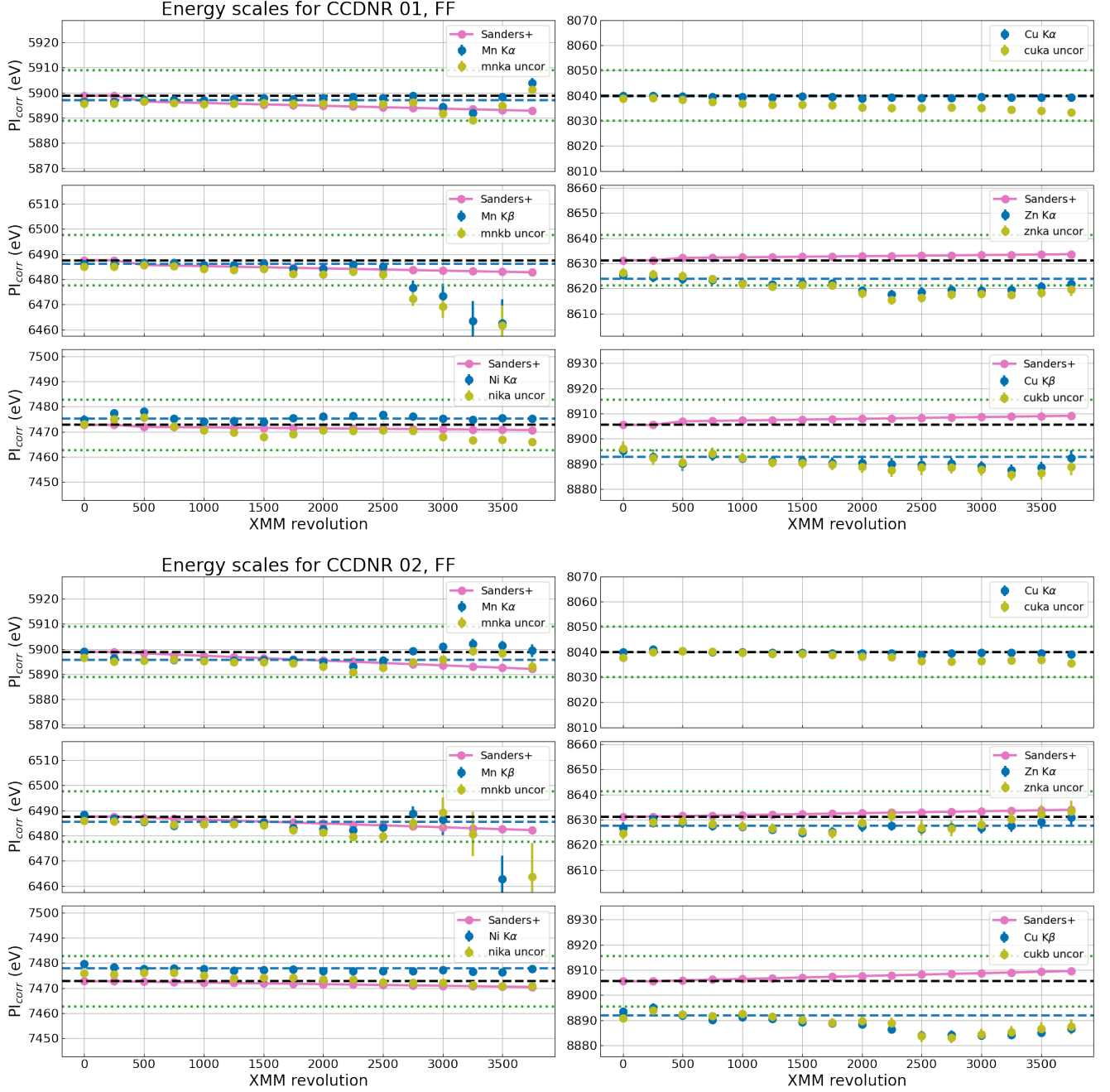


Figure 9: Energy scale for CCDNR01 (top) and CCDNR02 (bottom) in FF mode, after applying the second-step correction (spatial CTI). The data points (blue dots) are the best-fit line energies after the spatial CTI correction, olive points are before the correction. The black dashed line is the reference line energy, the blue dashed line is the median of the fitted line energies using the first 5 stacks data points (rev ≤ 1000), the green dotted lines are at ±10 eV around the reference energy of the line. The S20 time-dependent energy scale correction, averaged for the full CCD area, is shown with pink curves. Note that the data points (blue and olive dots) are not statistically independent as there is 250 revolution overlap, except for the first and the last ones.

Figure 10: See caption for Fig. 9. Note that the long-term CTI for Mn lines in CCDNR 04 is optimised for the boresight (RAWY > 180) while here the fit is performed over the full CCD.
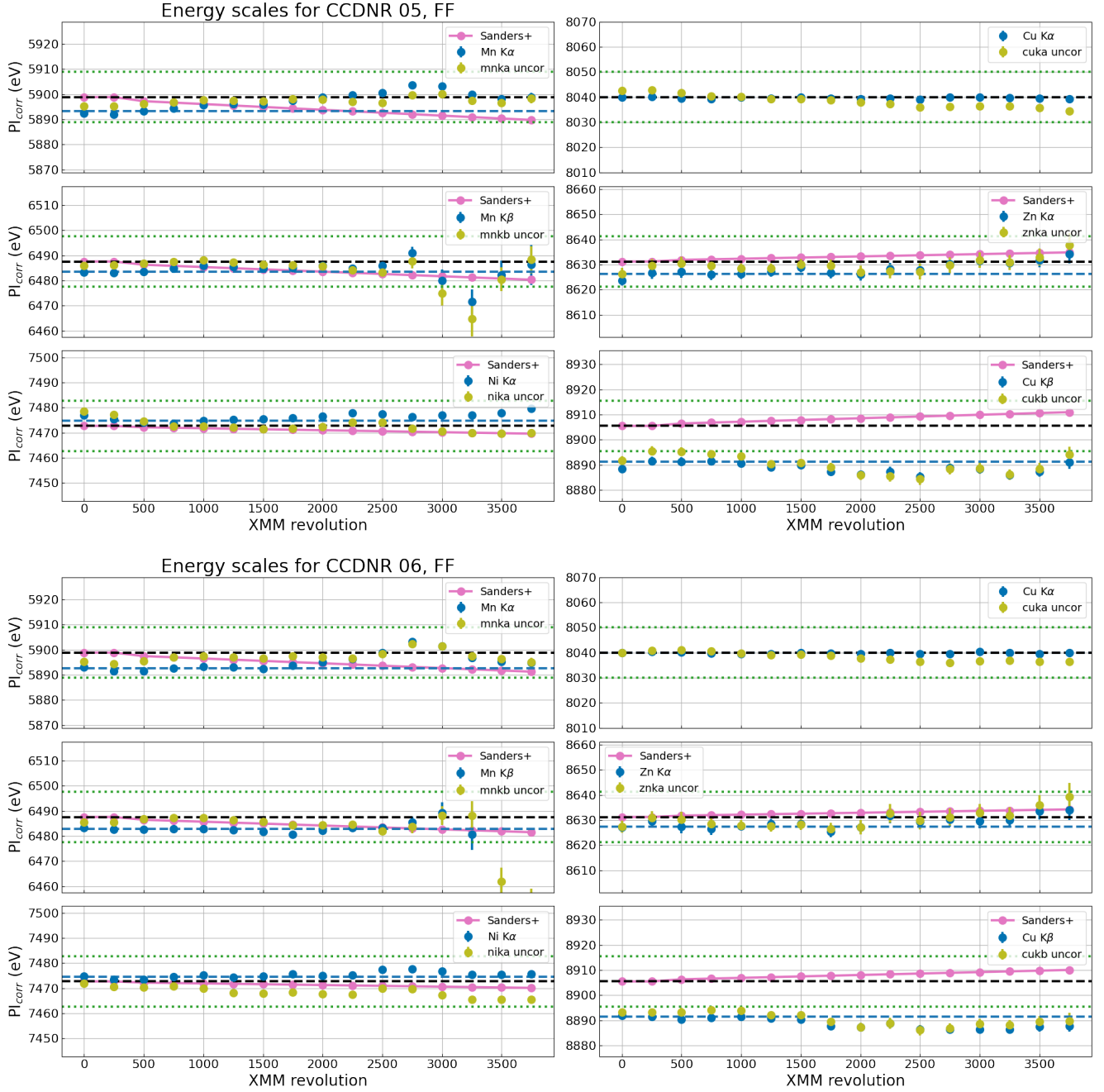
Figure 11: See caption for Fig. 9.
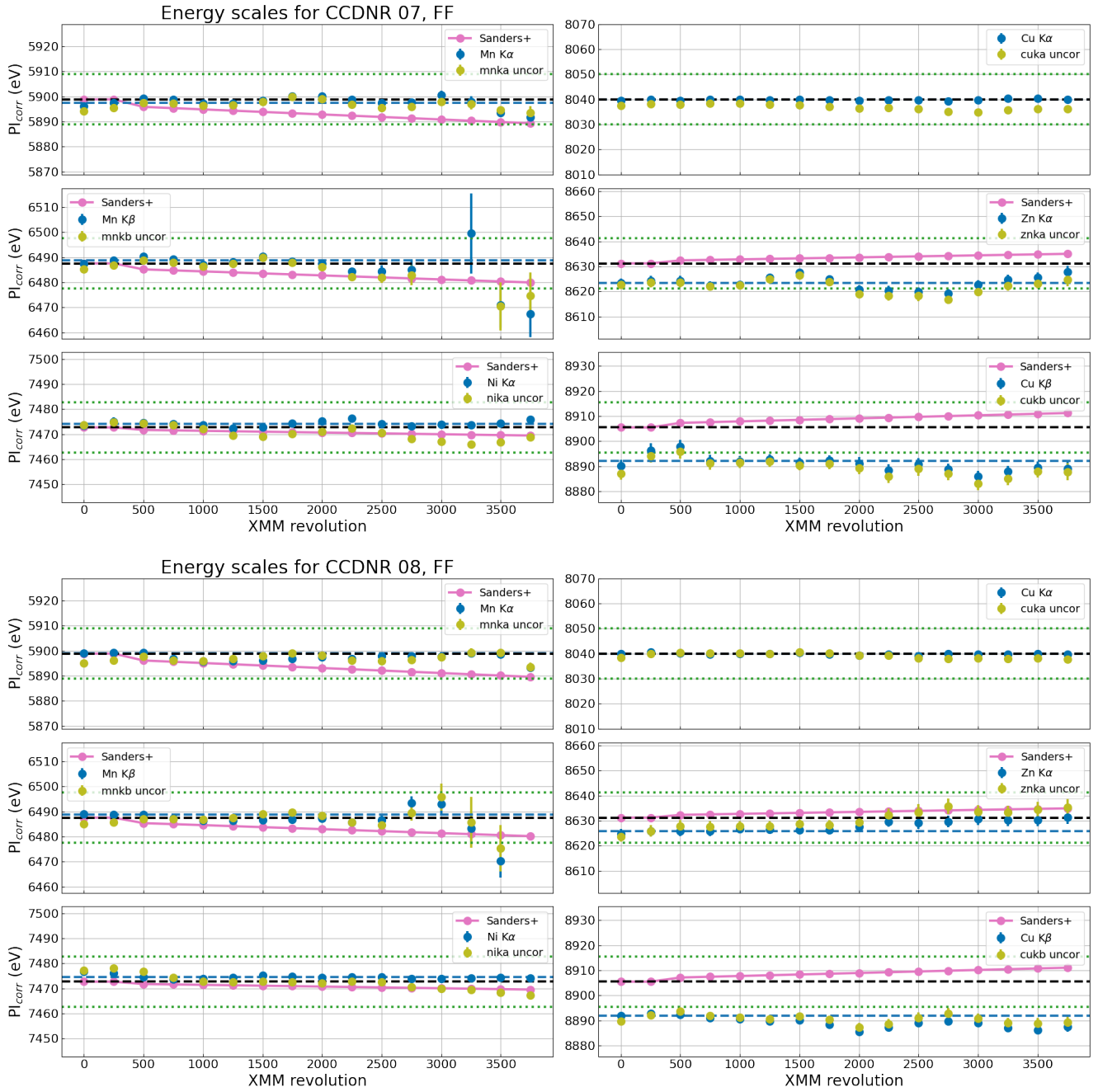
Figure 12: See caption for Fig. 9.
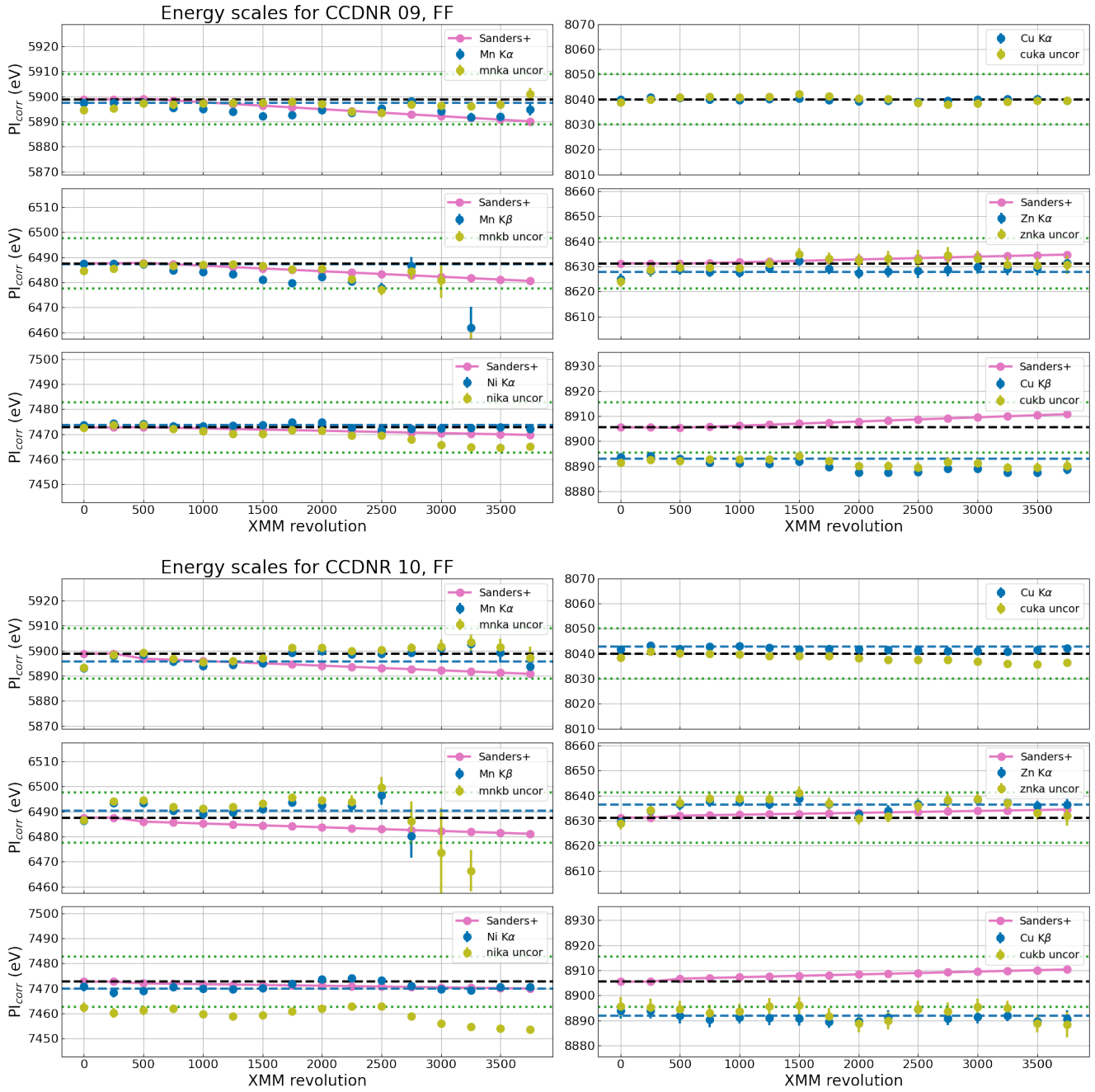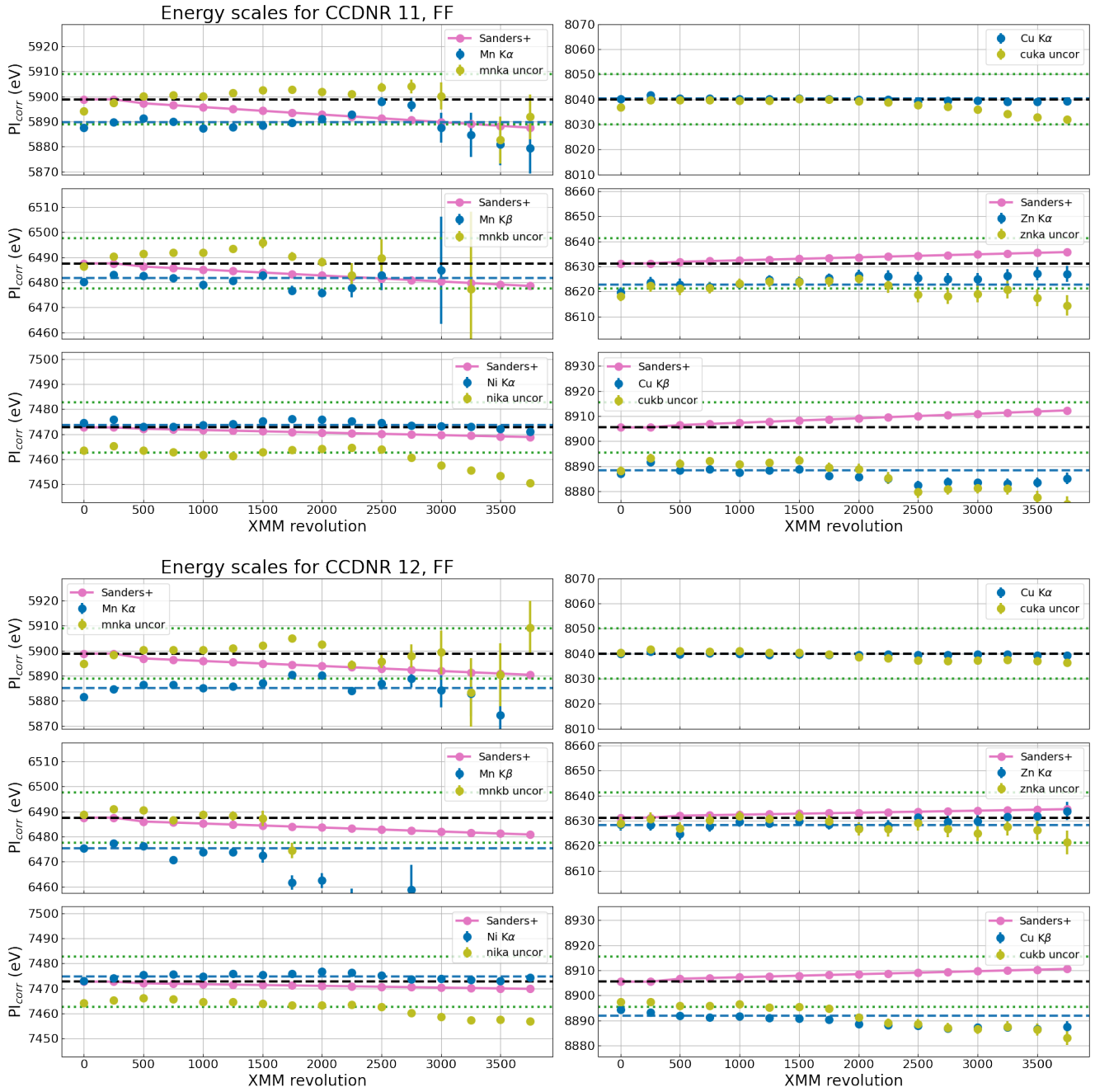
Figure 13: See caption for Fig. 9.

Figure 14: See caption for Fig. 9.

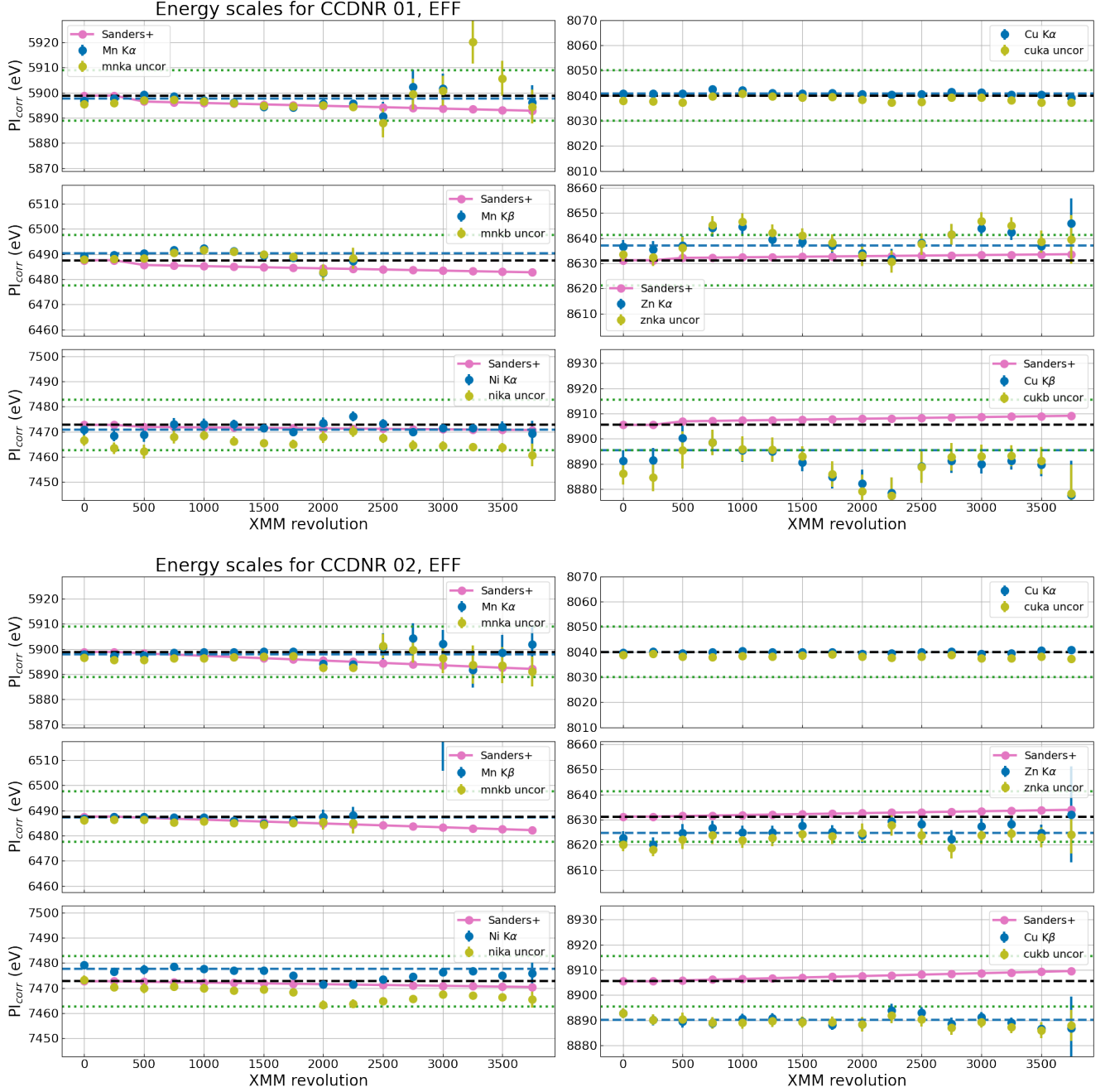# D    Energy scale results for EFF mode and all CCDs



Figure 15: Energy scale for CCDNR01 (top) and CCDNR02 (bottom) in EFF mode, after applying the second-step correction (spatial CTI). The data points (blue dots) are the best-fit line energies after the spatial CTI correction, olive points are before the correction. The black dashed line is the reference line energy, the blue dashed line is the median of the fitted line energies using the first 5 stacks data points (rev ≤ 1000), the green dotted lines are at ±10 eV around the reference energy of the line. The S20 time-dependent energy scale correction, averaged for the full CCD area, is shown with pink curves. Note that the data points (blue and olive dots) are not statistically independent as there is 250 revolution overlap, except for the first and the last ones.
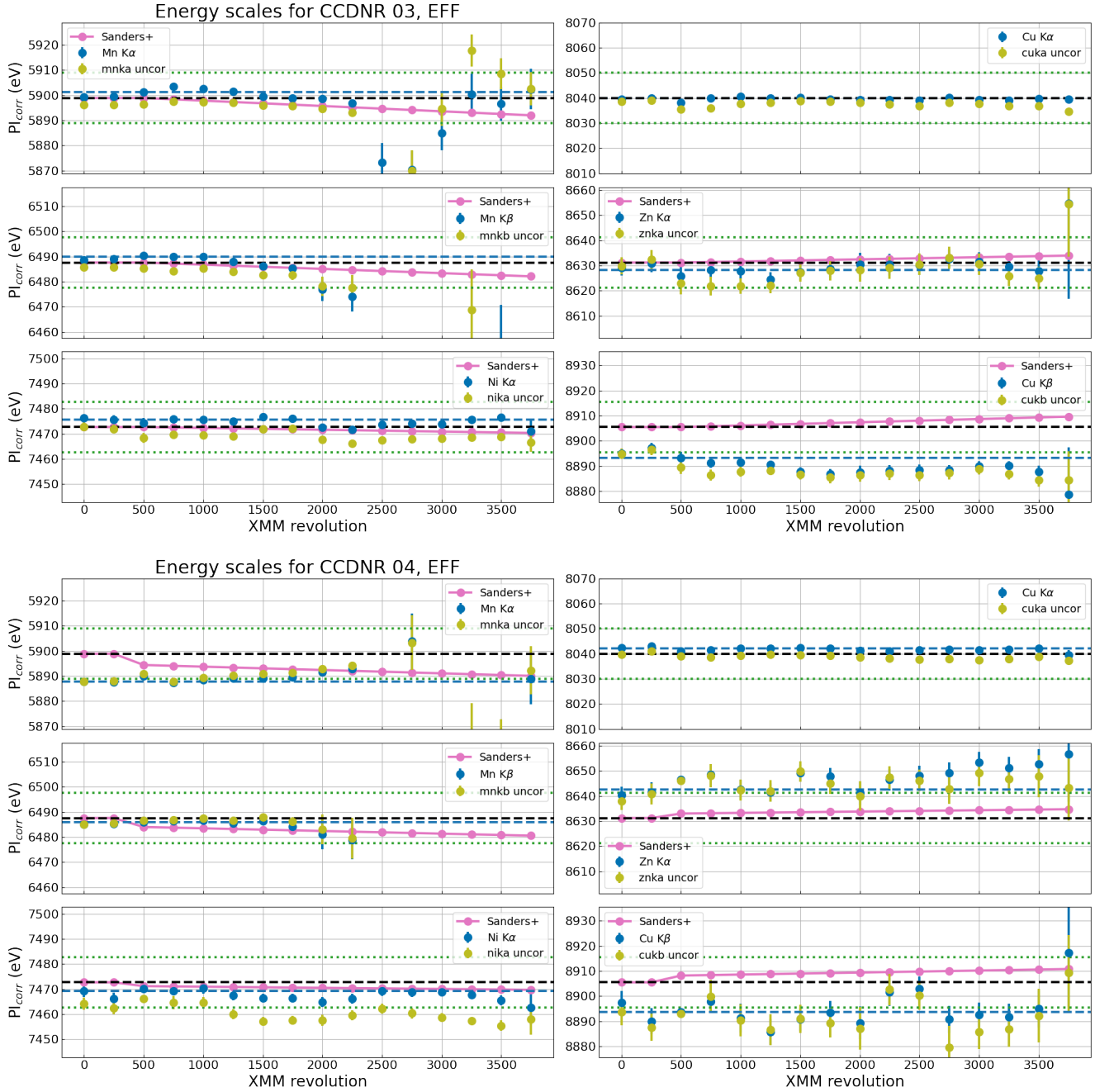
Figure 16: See caption for Fig. 15. Note that the long-term CTI for Mn lines in CCDNR 04 is optimised for the boresight (RAWY > 180) while here the fit is performed over the full CCD.
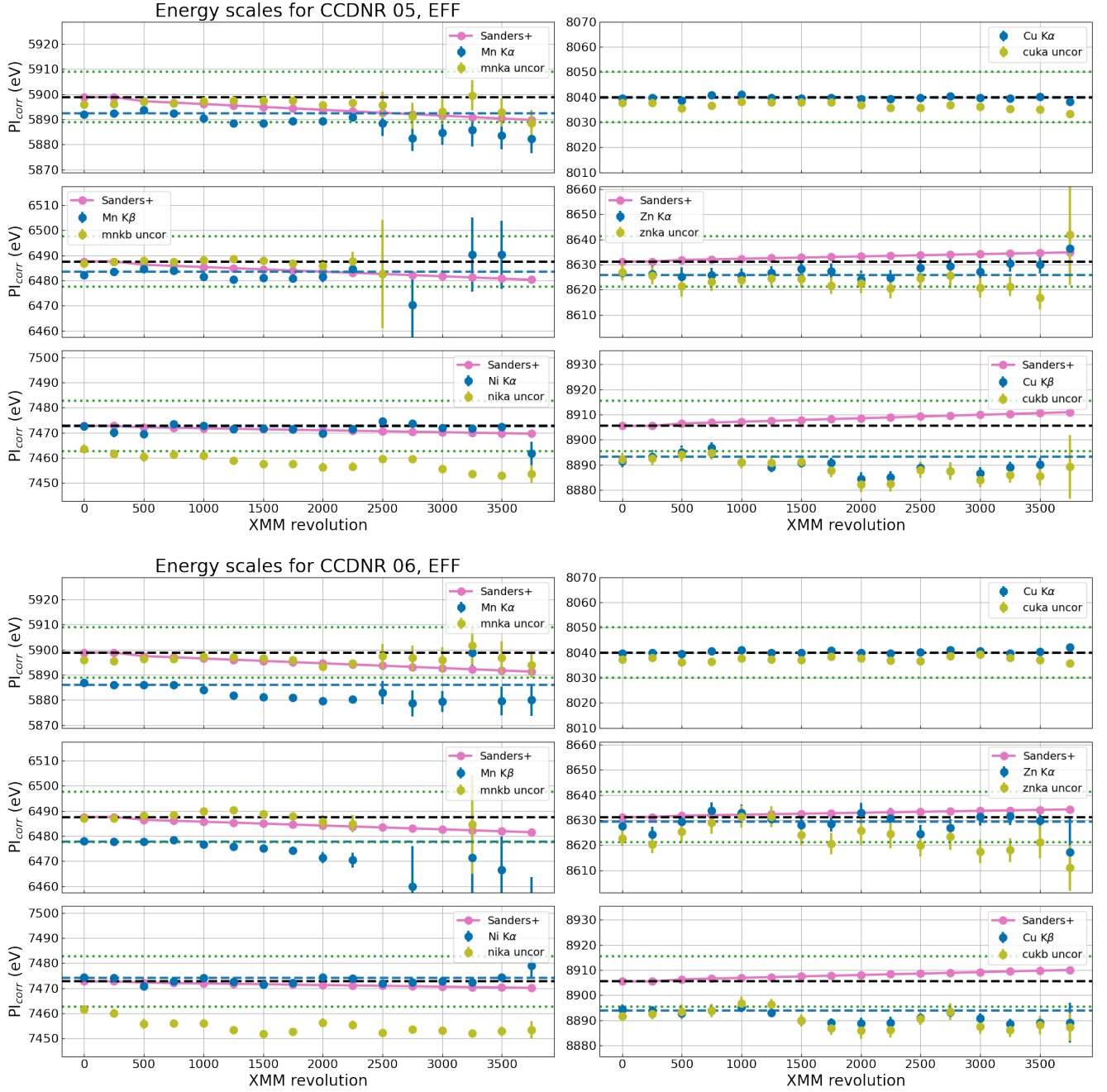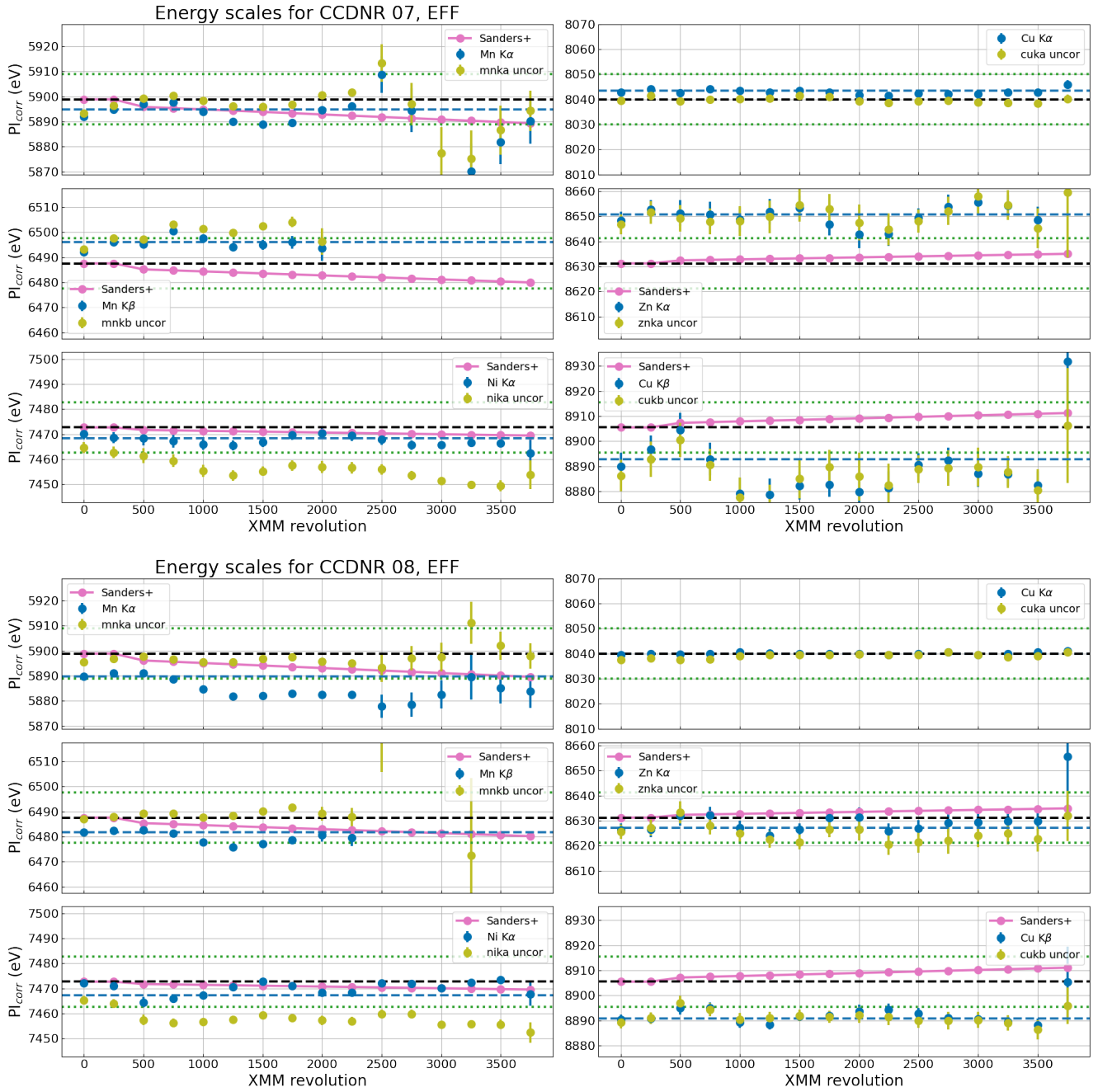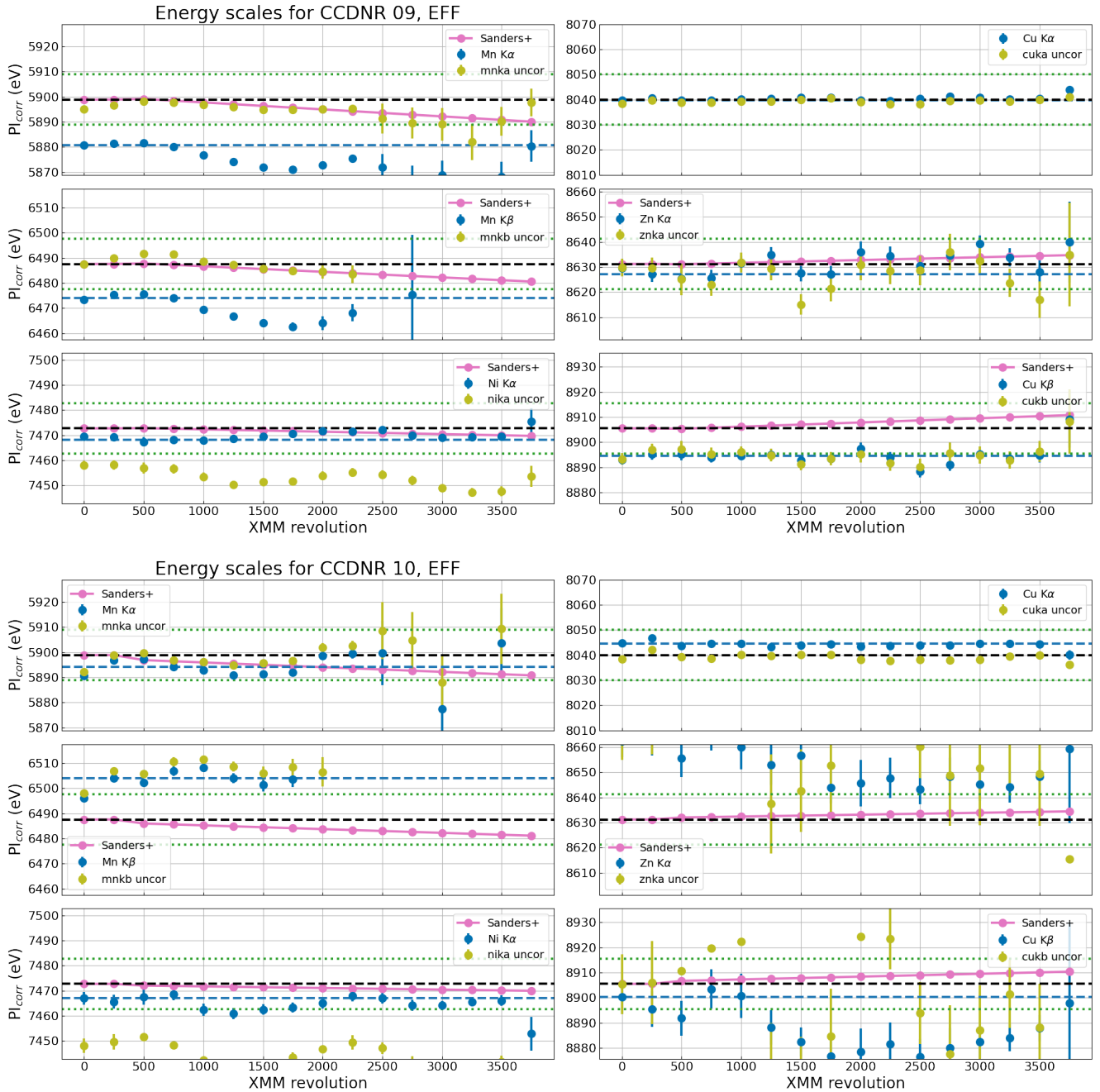
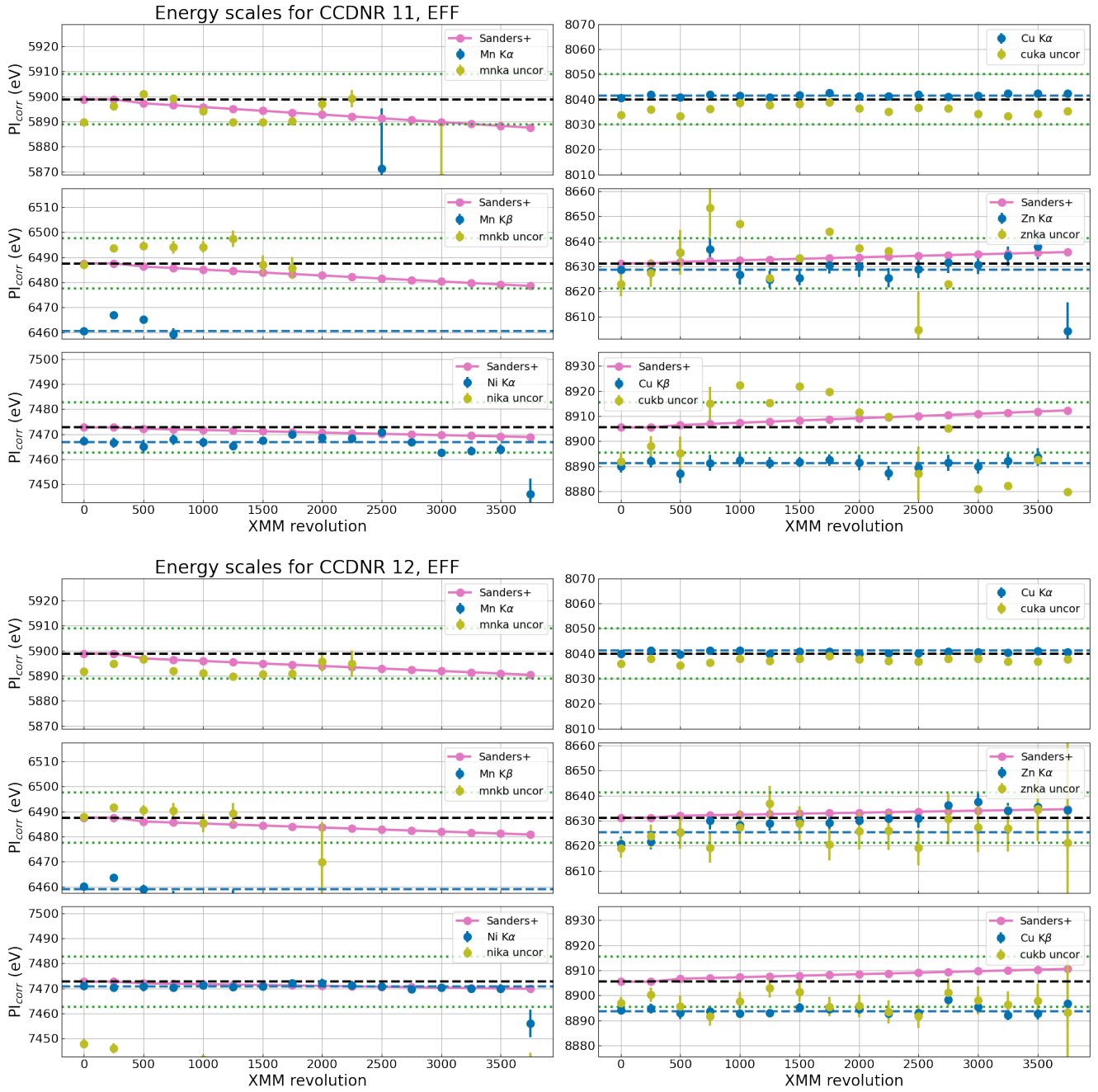Figure 17: See caption for Fig. 15.

Figure 18: See caption for Fig. 15.

Figure 19: See caption for Fig. 15.

Figure 20: See caption for Fig. 15.